An asymmetric upwind flow, Yellow Sea Warm Current: 1. New observations in the western Yellow Sea

Xiaopei Lin,[1] Jiayan Yang,[2] Jingsong Guo,[3] Zhixin Zhang,[3] Yuqi Yin,[1] Xiangzhou Song,[1,2] and Xiaohui Zhang[1]

Received 9 July 2010; revised 5 February 2011; accepted 11 February 2011; published 29 April 2011.

[1] The winter water mass along the Yellow Sea Trough (YST), especially on the western side of the trough, is considerably warmer and saltier than the ambient shelf water mass. This observed tongue-shape hydrographic feature implies the existence of a winter along-trough and onshore current, often referred to as the Yellow Sea Warm Current (YSWC). However, the YSWC has not been confirmed by direct current measurements and therefore skepticism remains regarding its existence. Some studies suggest that the presence of the warm water could be due to frontal instability, eddies, or synoptic scale wind bursts. It is noted that in situ observations used in most previous studies were from the central and eastern sides of the YST even though it is known that the warm water core is more pronounced along the western side. Data from the western side have been scarce. Here we present a set of newly available Chinese observations, including some from a coordinated effort involving three Chinese vessels in the western YST during the 2006–2007 winter. The data show unambiguously the existence of the warm current on the western side of YST. Both the current and hydrography observations indicate a dominant barotropic structure of YSWC. The westward deviation of YSWC axis is particularly obvious to the south of 35°N and is clearly associated with an onshore movement of warm water. To the north of 35°N, the YSWC flows along the bathymetry with slightly downslope movement. We conclude that the barotropic current is mainly responsible for the warm water intrusion, while the Ekman and baroclinic currents play an important but secondary role. These observations help fill an observational gap and establish a more complete view of the YSWC.

Citation: Lin, X., J. Yang, J. Guo, Z. Zhang, Y. Yin, X. Song, and X. Zhang (2011), An asymmetric upwind flow, Yellow Sea Warm Current: 1. New observations in the western Yellow Sea, *J. Geophys. Res.*, *116*, C04026, doi:10.1029/2010JC006513.

1. Introduction and Background

[2] The Yellow Sea (YS) is a broad shelf sea in the northwestern Pacific Ocean. A noticeable bathymetric feature is a trough that extends northwestward from the continental slope toward the Bohai Sea (BS), a semienclosed basin bordered by a coastline with a cluster of major metropolitan centers. In winter the water mass along the central and western side of the Yellow Sea Trough (YST) is distinctly warmer and saltier than the ambient water. This hydrographic feature suggests the existence of a northward winter current which flows against the prevailing northerly monsoonal wind (see Figure 1 for a schematic). This winter current, commonly called the Yellow Sea Warm Current (YSWC), is the main conduit by which the deep Pacific Ocean influences the BS and YS. The YSWC affects not only the hydrography and biogeochemistry of the shallow water in the region, but also maritime conditions, such as sea ice coverage, in some of the busiest harbors in the world [*Su et al.*, 2005]. Understanding the mechanism of the YSWC and its variability therefore has been a major focus of regional oceanographic investigations.

[3] The existence of the YSWC was first suggested by *Uda* [1934, 1936] based on the tongue-shape distribution of warm and salty water of Pacific Ocean origin. The schematic in Figure 1 is based on a collection of previous studies, including *Yuan and Su* [1984], *Guan* [1994], *Ichikawa and Beardsley* [2002], *Yuan et al.* [2008], and *Isobe* [2008]. To compensate YSWC transport, there are two southward coastal currents along the Chinese and Korean coasts. Other prominent currents in the region include the Tsushima Warm Current (TSWC) which flows into the Sea of Japan (East Sea) and the Taiwan Warm Current (TWC) which originates from the Taiwan Strait and the East China Sea shelf region (part of TWC water originates from the Kuroshio). These currents are interconnected and form a

[1]Physical Oceanography Laboratory, Ocean University of China, Qingdao, China.
[2]Department of Physical Oceanography, Woods Hole Oceanographic Institution, Woods Hole, Massachusetts, USA.
[3]Key Laboratory of Marine Science and Numerical Modeling, First Institute of Oceanography, State Oceanic Administration, Qingdao, China.

0148-0227/11/2010JC006513

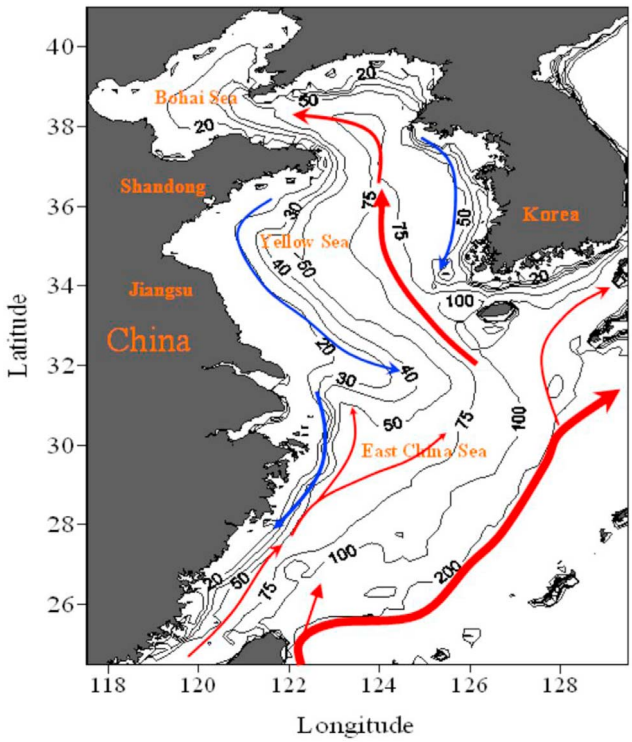

Figure 1. Schematic map of winter circulation in the Yellow Sea and East China Sea. The red arrows denote the warm currents and the blue arrows denote the cold currents. Black lines are the bathymetry with 50, 100, and 200 m labeled.

coastal warm current system in the East Asian Marginal Seas. In fact, historically, the YSWC was considered either as an upstream branch of the TSWC [*Nitani*, 1972; *Guan*, 1994; *Guan and Chen*, 1964] or as an extension of the perennially northward flowing TWC [*Beardsley et al.*, 1985]. However, the intrusion of the warm water along the YST is a winter-only feature [*Lie*, 1986; *Park*, 1986; *Beardsley et al.*, 1992; *Lie et al.*, 2000; *Guo et al.*, 2000; *Teague and Jacobs*, 2000], while the transport of both the TWC and the TSWC peak in the summer. Thus, in some studies the YSWC has been considered as a locally wind-driven flow or even as a sporadic response to strong northerly wind bursts [*Hsueh et al.*, 1986; *Hsueh*, 1988].

[4] *Lie et al.* [2001, 2009] questioned the existence of the YSWC by noting that the current has been inferred from the T-S distribution rather than verified by direct current measurements. They found a thermal front to the west of Cheju Island and argued that this would block the intrusion of warm water into the southern Yellow Sea. A noteworthy result from their study is that the along-trough velocity was very weak in all direct current measurements that were available to them. They concluded, therefore, that the YSWC is an intermittent upwind flow which occurs when the western front of the Cheju Warm Current collapses during northerly wind bursts. Other studies, like *Xie et al.* [2002], also suggested the tongue shape distribution of warm water is not necessarily due to advection of warm water. They argued that the surface cooling and subsequent convective mixing in winter could lead to a warm water presence along the trough due to the larger depth-integrated heat capacity in deeper regions.

[5] Most observations that have been discussed in the literature, including those by *Lie et al.* [2009], were made in the central YS or on the eastern side of the YST. While in situ data on the western side of the YST are rarely available, the observations have shown that the core of the warm water is distributed along the western YST [e.g., *Tang et al.*, 2001; *Huang et al.*, 2005]. It would be difficult to fully reconcile assessments and hypotheses derived from different observations without data on the western side. So a more systematic description of YSWC needs observations on the western YST.

[6] During the winter of 2006–2007, a comprehensive observational program with coordinated cruises of three research vessels was made by Chinese oceanographers on the western side of the YST. This survey was conducted jointly by the Ocean University of China (OUC) and the First Institution of Oceanography, State Oceanic Administration (FIO). The observations filled a large void in the available data and provide a more complete data-based description of oceanic conditions in the YS, especially on western side of the YST. The main purpose of this study is to use this new set of observations, along with previously available in situ and satellite data, to update the characterization of the YSWC. Our study shows that a steady northward YSWC indeed exists in the wintertime, but its axis is shifted upslope toward the western side of the trough. This could potentially explain why the current was weak along the central trough in the data analyzed by *Lie et al.* [2009].

[7] The paper is organized as follows. The data set used in this study is introduced in section 2. We present analyses the newly observed YSWC features in section 3. A discussion and a summary are given in sections 4 and 5.

2. The Data

2.1. The 2006–2007 Winter Investigation

[8] Between 21 December 2006 and 14 February 2007 a large-scale survey involving three research vessels was conducted in a coordinated effort by Chinese oceanographers to study the western Yellow Sea. Three research vessels were used simultaneously. There were 464 stations with interstation distances less than 20 km. During the observations, several outbreaks of strong northerly wind with cold airs occurred, e.g., on 28 December 2006, 8 January 2007, and 28 January 2007. The field work was suspended during each storm event which typically lasted for about 2–3 days. Among all stations, 110 of them were along the coast of Shandong and Jiangsu Provinces. The observation was made prior to 10 January 2007 in these costal stations. We exclude data from those 110 coastal stations in the present study since they were not located in the vicinity of the YST. The remaining 354 stations were located on the western YST (Figure 2) and are used in this study. Observations in all of them were made between 10 January and 4 February 2007. At each station, temperature and salinity were measured with a high vertical resolution of less than 0.1 m using Sea Bird

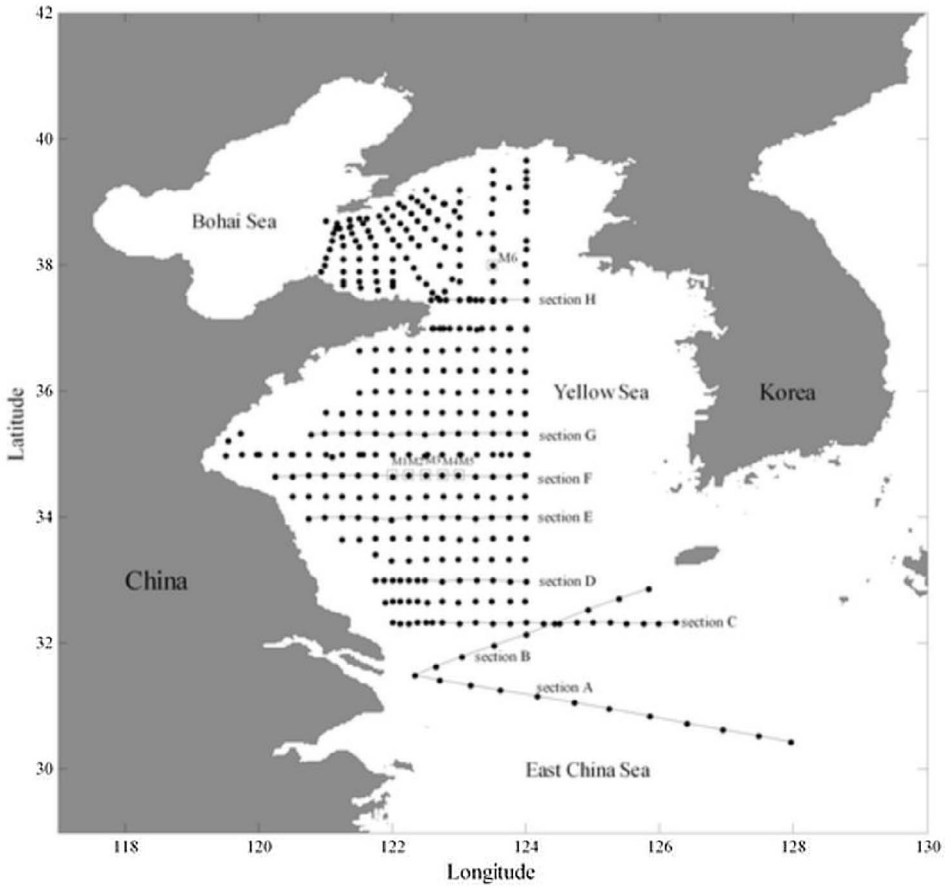

Figure 2. Stations from the 2006–2007 winter survey. Dots denote the field observation stations. Eight sections, named A-H, are selected to show the position of YSWC in different regions. The mooring stations, named M1–M6, are outlined by squares.

CTDs. All instruments were calibrated prior to and after the deployments following the standard procedures. Data with obvious biases were removed. In addition to CTD casts, 6 moorings with ADCPs were deployed along the possible pathway of the YSWC (Figure 2). FIO deployed moorings M1 to M5 in a section along 34.7°N (section F) in water depths ranging from 50 m to 70 m; the results showed the first direct evidence of the YSWC on the western side of the YST [*Yu et al.*, 2010]. OUC deployed mooring M6 in the northern end of the YST where the depth was 66 m. Unfortunately, the instruments from 2 mooring stations (M1, M3) were lost, likely due to the heavy fishing activity in the area. At each mooring site, a tide gauge and an upward looking 300 KHz RDI ADCP (Acoustic Doppler Currents Profile) or 250 KHz Sontek ADCP were deployed. The sampling interval was 5 min and bin size was 2 m in the vertical. Detailed information about the moorings is listed in Table 1. This observational program was likely the most comprehensive ever conducted on the western side of the YS.

2.2. Routine Section Data

[9] In addition to the 2006–2007 cruise data, we analyzed routine section observations made along 34°N, 35°N, and 36°N. The State Oceanic Administration (SOA) maintained these sections as routine surveys from 1976 to 2007. Each section was surveyed at least 4 times per year, including one in winter [*Guo et al.*, 2004]. These transects consisted of about 30 fixed stations for a period of more than 30 years.

Table 1. The Mooring Stations

Station	Latitude (°N)	Longitude (°E)	Depth (m)	Start Day	End Day	Bin Size (m)
M1	34°40.04′	121°59.84′	51	9 Dec	23 Jan	2
M2	34°40.35′	122°15.06′	55	9 Dec	23 Jan	2
M3	34°40.53′	122°29.74′	62	9 Dec	23 Jan	2
M4	34°40.21′	122°45.48′	71	9 Dec	23 Jan	2
M5	34°40.01′	123°00.49′	73	9 Dec	23 Jan	2
M6	38°00.53′	123°30.67′	66	31 Dec	8 Feb	2

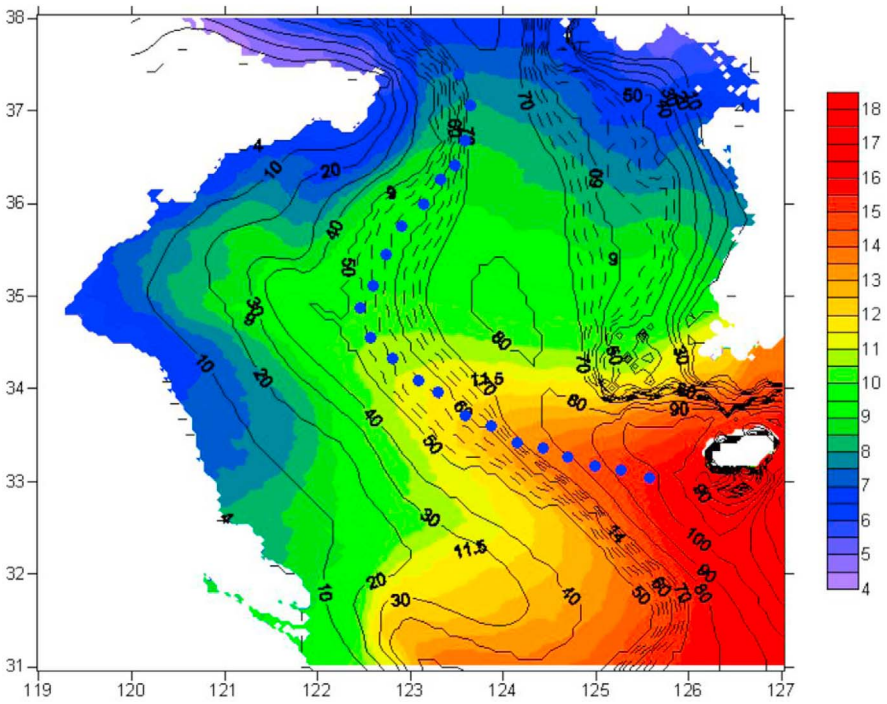

Figure 3. The mean SST (°C) in winter (DJF) from AVHRR observations from 1985 to 2009. The blue dots denote the axis of warm water tongue as the pathway of YSWC. The black lines are the bathymetry with the dashed lines representing the 2.5 m interval between 50 and 70 m.

2.3. Sea Surface Temperature and Wind Stress Data

[10] The sea surface temperature (SST) data set used here was the 4 km × 4 km monthly average PFSST based on the Pathfinder algorithm for the period from January 1985 to February 2009. The data were derived from the five-channel advanced very high resolution radiometers (AVHRRs) on board the NOAA −7, −9, −11, −14, −16, −17 series of polar orbiting satellites and combined with the in situ buoy data. This is a newer version of SST product from NOAA/NASA AVHRR Oceans Pathfinder Program. The earlier version on the 9.28 m grid [*Kilpatrick et al.*, 2001] has been applied in the Bohai Sea, Yellow Sea and East China Sea. *Gao et al.* [2001] compared the 9.28 km PFSST with in situ data in this region and found that in 67.6% of all data pairs, the difference is less than or equal to 0.5 K, and the root mean square error for all pairs is about 0.61 K. The newly published Pathfinder V5 data set provides even higher resolution (4 × 4 km) and presumably a more accurate SST product than the earlier version. For this study, the Yellow Sea surface temperature between 31°N and 38°N and 119°E and 127°E, in each winter (DJF) from 1985 to 2009 were extracted from the PFSST data set. Based on a hierarchical suite of tests [*Kilpatrick et al.*, 2001], the SST quality varies from 0 to 7, with 0 being the lowest quality and 7 being the highest quality. Pixels with quality from 5 to 7 were selected and used to interpolate in those pixels with low-quality data.

[11] If the YSWC is a locally wind-driven current, its existence and variability should be highly correlated with wind stress forcing. In this study, we used the QuikSCAT daily sea surface vector wind [*Liu*, 2002] coincident with the 2006–2007 winter cruises. The wind data have a resolution of 1/4° in both longitude and latitude.

3. The Observed YSWC

[12] Observations from the 2006–2007 winter cruises and other data are used here to characterize the structure and variability of the YSWC. These data are presented and discussed in this section.

3.1. Upslope and Westward Shift of the YSWC

[13] As noted previously, the intrusion of warm water is not exactly along the central YS trough axis but is displaced westward. This can be seen in the SST field from satellite AVHRR sensors. Figure 3 shows the mean winter SST averaged from 1985 to 2009. The axis of the warm water, denoted by blue dots and defined by the maximum SST across the trough, is clearly displaced westward. South of 35°N, the upslope movement of warm water tongue is very obvious. The axis of warm water (blue dots) is heading northwestward from the water depth of more than 100m in 32°N to about 70m in 33°N. Between 33°N to 35°N, the cross-shelf and onshore intrusion is gradual from 70m to about 50m. The warm water axis reaches the most western position of about 122.5 °E in 35°N. To north of 35°N, the warm water intrusion is basically along the bathymetry with slightly downslope movement. There is another warm water tongue heading northwest toward the Shandong coast line, along the divergence of topography. This westward displacement of the YSWC has been pointed out in several previous studies. For instance, *Tang et al.* [2001] showed

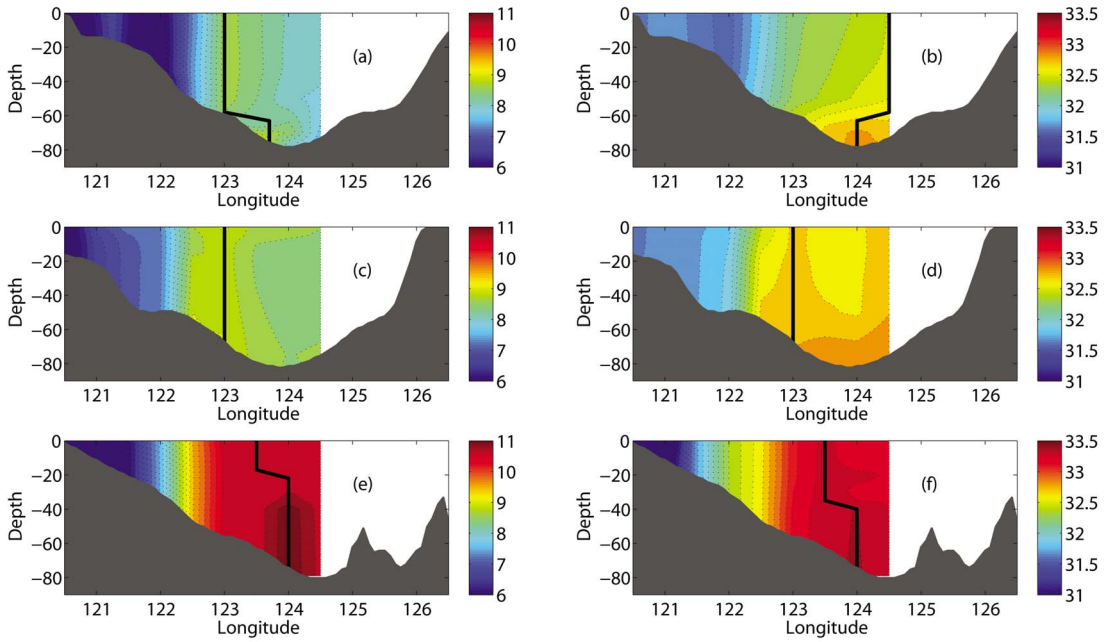

Figure 4. The average (1976–2007) winter temperature (°C) from three routine sections, (a) 36°N, (c) 35°N, and (e) 34°N, and salinity (psu) from three routine sections, (b) 36°N, (d) 35°N, and (f) 34°N. The temperature interval is 0.2°C and salinity interval is 0.1 (dashed line). The maximum temperature and salinity are labeled by the black bold line.

clearly the presence of high temperature and salinity anomalies on the western part of the YST in winter. A more recent study by *Ma et al.* [2006] found the double warm tongues in the Yellow Sea in winter, with an intermittent tongue along the central trough and a persistent tongue on the western side. *Xie et al.* [2002] also noticed the westward shift of the warm water and speculated that the westward Ekman flow may be responsible for the shift. *Huang et al.* [2005] suggested that the westward shift could be due to the surface cooling and self-advection of baroclinic currents even though it was noted that the barotropic current in their 3-D model was responsible for the westward shift of the warm tongue.

[14] The displacement of the warm water occurred not only in the SST field but also over the water column. This was revealed in the hydrographic sections along 34°N, 35°N, and 36°N from the SOA routine surveys from 1976 to 2007. The 31 year average winter observations (Figures 4a, 4c, and 4e) show that the whole water column, not merely the top Ekman layer, was warmer and saltier on the western side of the trough. The warm water column (black bold line denotes the axis) actually slightly moved upslope from 34°N to 35°N but downslope from 35°N to 36°N. This pattern is consistent with the path of the YSWC from satellite observations in Figure 3. Another important evidence for the existence of YSWC is the tongue of high salinity (Figures 4b, 4d, and 4f), which is also located in the western YST along with the warm water core. So the presence of a warm/salty water column on the western side of the YST was evident climatologically in this 31 year record. High salinity in the warm water tongue may compensate the temperature effect and thus reduce the thermal wind shear in the baroclinic geostrophic velocity. It is interesting to note that there was a high temperature core on the bottom just to the west of the trough at 34N, 124E (Figure 4e). This temperature inversion was accompanied by a negative salinity gradient in vertical (Figure 4f) and so water remained stably stratified. While the salinity was distinctly higher in the warm water column in all three sections, there was a considerable vertical stratification in salinity along all three sections. This contrasts with a vertically more uniform temperature profile. The salinity stratification suggests that intense surface-to-bottom vertical mixing, as hypothesized by *Xie et al.* [2002], does not play the leading role in setting the winter hydrographic structure along the trough. Lateral advection was more likely responsible for the existence of the warm and salty water column. Geostrophic velocity and its vertical shear over the whole water column are strongly steered by bathymetry on a f plane even when the water is strongly stratified [*Brink*, 1998]. It is therefore expected that geostrophic component of the YSWC could preserve its T-S stratification from the upstream. Ageostrophic velocity components, like surface and bottom Ekman layer velocity, are certainly important as well as to be shown in the velocity data.

3.2. The Winter Observations in 2006–2007

[15] Figure 4, based on three routine hydrographic surveys, clearly shows that the warm and salty water mass is located on the western YST. Prior to the observational program described here, the structure of the western side of the YSWC was ambiguous and the existence of the YSWC

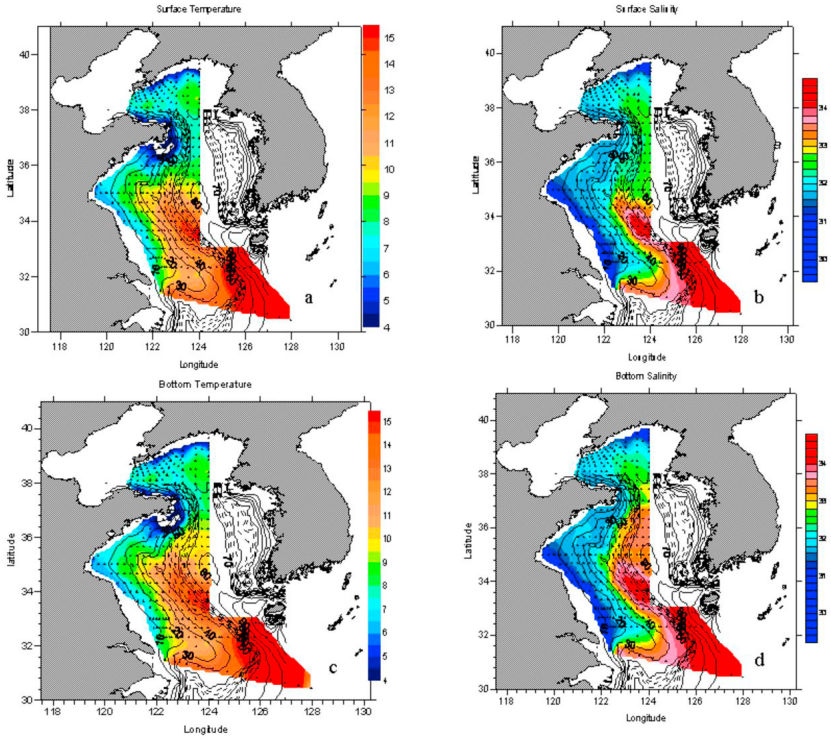

Figure 5. Maps of water properties from the 2006–2007 winter survey with temperature in °C and salinity in psu. They are the (a) surface temperature, (b) surface salinity, (c) bottom temperature, and (d) bottom salinity. Dots denote the stations. Water depths of 10, 30, 50, 70, and 90 m are labeled with black lines with the dashed lines representing the 2.5 m interval between 50 and 70 m.

remained to be confirmed by direct current measurements. The data from the 2006–2007 cruises helped close some gaps in knowledge of the YSWC.

[16] Maps of surface and bottom temperature and salinity during the winter of 2006–2007 are shown in Figure 5. High temperature and salinity water is clearly seen on the western side of the trough from surface to the bottom and this is consistent with the three time average winter vertical sections shown in Figure 4. The main feature in the maps is a warm and salty water tongue trending northward from the

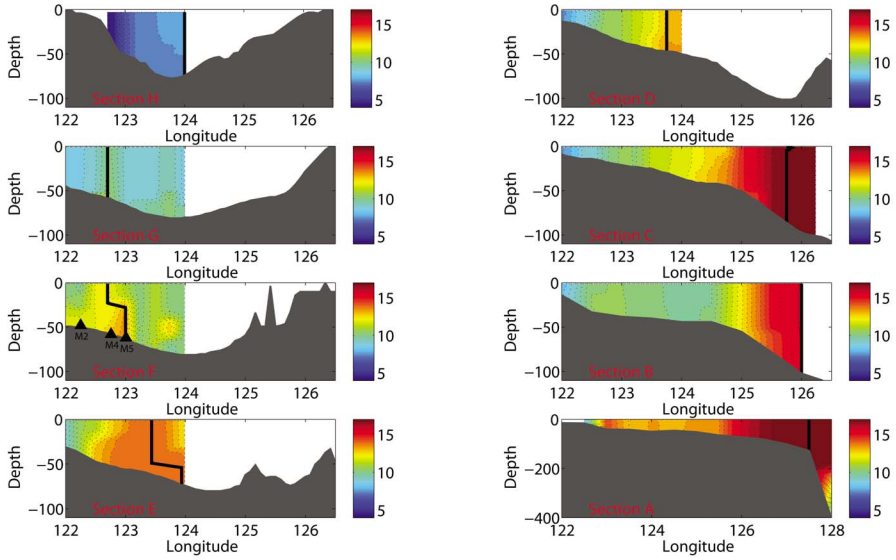

Figure 6. The temperature (°C) in sections A-H with interval of 0.2°C (dashed line). The maximum temperature is shown with the black bold line. The position of the sections is shown in Figure 2.

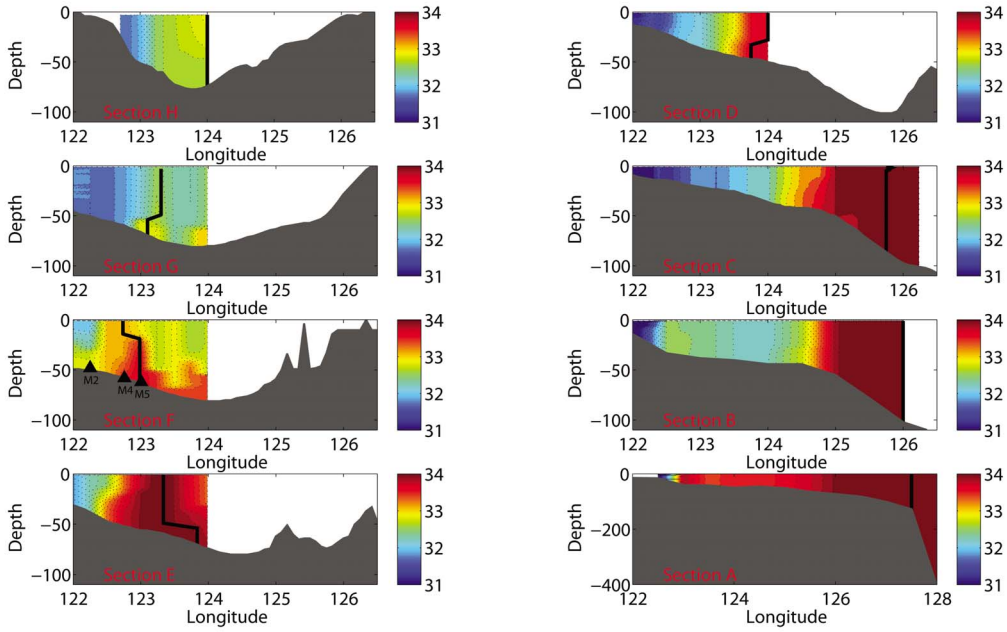

Figure 7. The same as Figure 6 but for salinity (psu). The interval is 0.1.

southern YS toward the BS, indicating the pathway of YSWC. South of 35°N, the warm and salty water trends northwestward from the central trough to the western slope, indicating cross-isobathic water movement. North of 35°N, the water tongue turns northeastward, basically along the 50–70 m isobaths, eventually reaching the BS. We also notice the existence of a second warm and salty water tongue toward the Shandong coastal line from 35°N to 36°N. This water intrusion is roughly along the divergence of bathymetry and more obvious in temperature than in salinity. Westward and cross-isobathic movement south of 35°N, is also suggested in Figures 6 and 7, which show vertical temperature and salinity sections from the southern to northern Yellow Sea. Along section A, the axis (black bold line) of warm and salty water with temperature greater than 16°C and salinity higher than 34 was located in about 127.5°E, where the water depth is 165 m. Along sections B and C (32.3°N), the warm and salty water core was near the central trough with water depth more than 100m. The easternmost stations along sections A, B, and C were in the shelf break region and can be considered as the entrance of the YSWC into the YST. At those stations with temperature higher than 15°C and salinity higher than 34, the water was most likely from the Kuroshio or Taiwan Warm Currents. Due to the lack of observations east of 124°E along section D, we cannot determine the warm/salty water axis precisely; however it does appear that the core of YSWC water moved westward. The westward and onshore movement of warm/salty water core becomes obvious from sections E to G. The water axis moved from the center to the west slope of the trough where the depth is about 50–70 m. The warm temperature axis reached as far west as 122.7°E along section G, while the high-salinity axis was located in about 123°E. The discrepancy between temperature and salinity distribution in this region was also shown in Figures 4a and 4b (36°N section) and Figure 5. The salinity in this region is likely to be influenced by the fresh coastal water flowing outside of the BS along the Shandong coastal line. Data available to this study are insufficient to quantify the impact from the coastal current. A modeling study would be desirable but is beyond the scope of this study. North of section G, the warm and salty water tongue moved northeastward along the bathymetry. The temperature and salinity distribution were rather similar as that shown in Figure 4. The bottom water was warmer and saltier than the surface water along the trough. This feature can be traced to the upstream region around 31N. This further supports the YSWC moves upstream likely as a stratified Taylor column as discussed by *Brink* [1998] for a more general coastal flow. There was a second warm/salty water core on sections F and G in the central trough, which is was also reported by *Ma et al.* [2006]. We speculate that the local topography divergence was responsible for the presence of second warm/salty water core on sections F and G. This could be further investigated with a regional ocean model. Figures 5, 6, and 7 show that the warm and salty water tongue in the YS progressively shifts westward as the intrusion penetrates further onshore in the south of 35°N. This is quite consistent with the satellite SST observations during the investigation. Although patchy, the warm water tongue of AVHRR SST in January 2007 trends northwestward and upslope in the south of 35°N (Figure 8).

4. Discussion

[17] Both the in situ observations and satellite SST measurements indicate the westward and onshore movement of

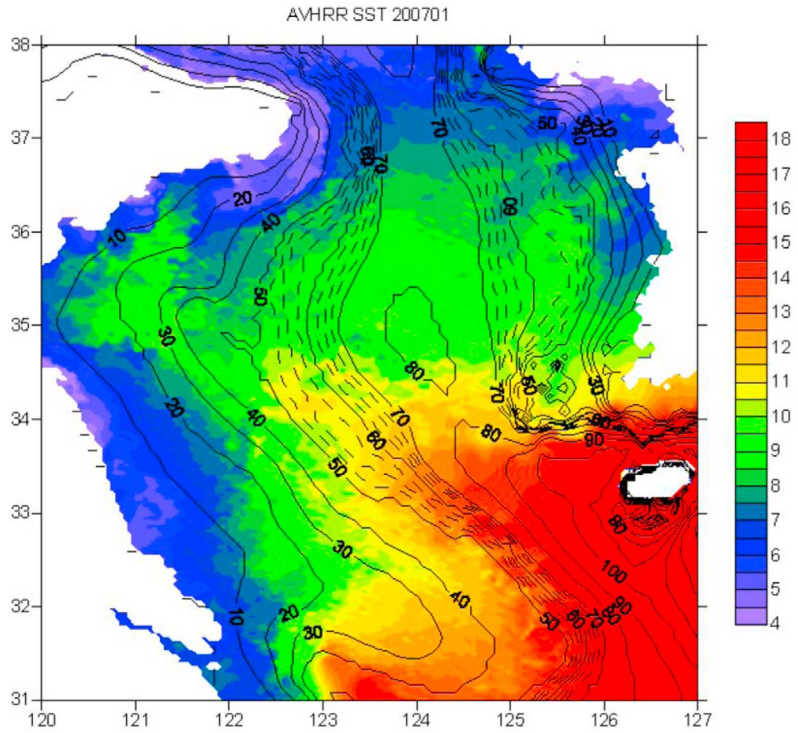

Figure 8. The mean SST (°C) in January 2007 from AVHRR observations. The black lines are the bathymetry with the dashed lines representing the 2.5 m interval between 50 and 70 m.

YSWC in the southern YS. These observations imply the existence of an onshore winter current along the western YST. To examine its existence, the residual currents at mooring stations M2, M4, M5, and M6 are used as the direct observation evidence of YSWC. These stations were located in the pathway of the warm and salty water tongue (Figure 2). Tides were removed from the ADCP data by Lanczos low-pass filtering [*Duchon*, 1979].

4.1. Mean Current at Morring Stations M2, M4, and M5

[18] Figure 9 shows the time-averaged currents at mooring stations M2, M4, and M5 with the background temperature of section F. The mean currents at stations M2, M4, and M5 are all directed to north or northwest from surface to bottom and support the existence of YSWC in the western YST. At M5, which was located near the warm water core in section F, the northwestward current speed was usually greater than 5 cm s^{-1}. The current speed at M2 and M4 were smaller and around 2–3 cm s^{-1}. There were strong vertical shear of velocity at M2 and M5, with westward in surface layer and northwestward in subsurface layer. This westward velocity component in both M2 and M5 indicates an upslope and onshore movement of YSWC as shown in the in situ and AVHRR SST observations. It is interesting that the currents at M4 had small shear and was basically northward in all layers.

4.2. The Ekman Model Used for Estimating Ekman Current

[19] To better understand the vertical structure of observed velocity field, **a** one-dimensional model is employed here to estimate the Ekman currents at the location of mooring stations. We want to discuss the contribution of Ekman, barotropic, and barocilinic current to the intrusion and shear of YSWC in the western trough. The wind forcing

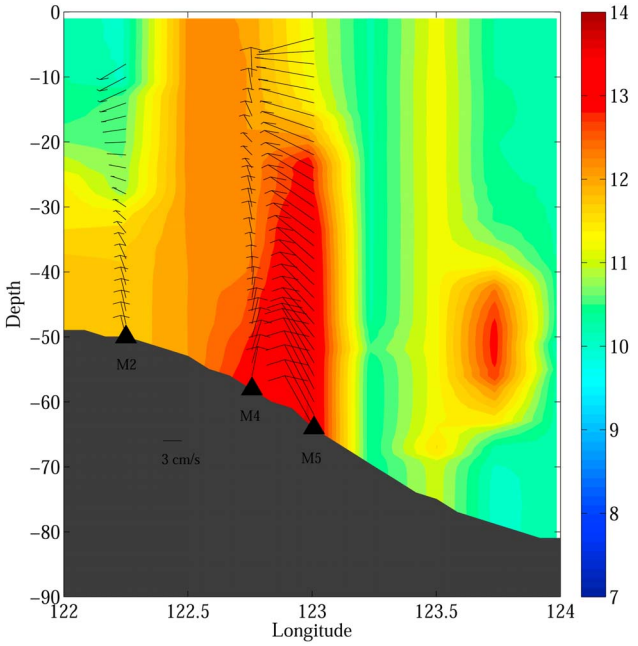

Figure 9. Time-averaged currents at mooring stations M2, M4, and M5 with the background temperature (°C) of section F.

Table 2. Parameters for the 1-D Ekman Model

Physical Parameter	Presentation	Value
Vertical resolution	z	2 m
Air density	ρ_a	1.23 kg m^{-3}
Wind drag coefficient	C_D	1.2×10^{-3}

is determined by the mean of adjacent nine grid points of QuikSCAT wind data during observation time in each mooring stations. The governing equation is

$$f \times \vec{u} = \nu \frac{\partial^2 \vec{u}}{\partial z^2},$$

where f is Coriolis parameter, $\vec{u}$ is the velocity, and ν is the viscosity. The surface boundary condition is

$$\rho_0 \nu \frac{\partial \vec{u}}{\partial z} = \vec{\tau},$$

where ρ_0 is the constant density derived from the mean density of each mooring station, and $\vec{\tau}$ is the surface wind stress from QuikSCAT observations, which is the same as the classic Ekman theory in the open oceans. In this calculation, ν is taken as 0.01 and other parameters are chosen according to *Price and Sundermeyer* [1999] as listed in Table 2. The results from the Ekman model will be used in the following discussions.

4.3. The Mean Residual, Ekman, Barotropic, and Baroclinic Components at Mooring Stations

[20] The three-dimensional residual current at mooring stations M2, M4, and M5 are shown in Figure 10a. The currents at M2 and M5 turn clockwise with the increasing of water depth and the current at M4 is basically northward in all the water depth with no obvious rotation. The rotation and shear of velocity field were associated with the Ekman and baroclinic current. Based on the estimated Ekman current in session 4.2, we decompose the residual currents in all the mooring stations into three components, Ekman current, barotropic current, and baroclinic current. The time-averaged Ekman current, barotropic current, and baroclinic current at M2, M4, and M5 are shown in Figures 10b, 10c, and 10d. The dominance of barotropic current is easy to see in all the three stations, compared with the Ekman current and baroclinic current. Considering the Ekman layer depth of about 20m in these mooring stations (Figure 10b), the Ekman currents are considerable only in the surface layer and not important in the subsurface layer. But the rotation and shear of velocity in M2 and M5 are from surface to bottom (Figure 10a). This rotation and shear were more likely associated with the baroclinic currents as indicating in Figure 10d. To estimate the relative importance of different component in the current field, the time-averaged barotropic current and its zonal and meridional components, depth-averaged Ekman current and baroclinic current are listed in Table 3 for the 3 mooring stations. The baroclinic velocity at M4 is the minimum among all the 3 moorings with only 1.21 cm s^{-1}. The relatively weak shear and rotation of velocity in M4 are due to the small baroclinic current component. In fact, Figure 9 shows that temperature has a large vertical gradient in both M2 and M5 but is nearly vertically uniform at M4. This may explain why the shear and rotation of velocity were weaker at M4. The barotropic currents were dominant at all the 3 mooring stations. At M5, which was located in the core of YSWC, the barotropic current speed was 7.76 cm s^{-1} with a westward (also in the onshore direction) component of 6.56 cm s^{-1}. Compared with the Ekman transport speed of 0.67 cm s^{-1} (the maximum Ekman current speed at surface is 4.10 cm s^{-1}) and the baroclinic current speed of 2.16 cm s^{-1}, the YSWC and its westward shift are dominated by the barotropic current.

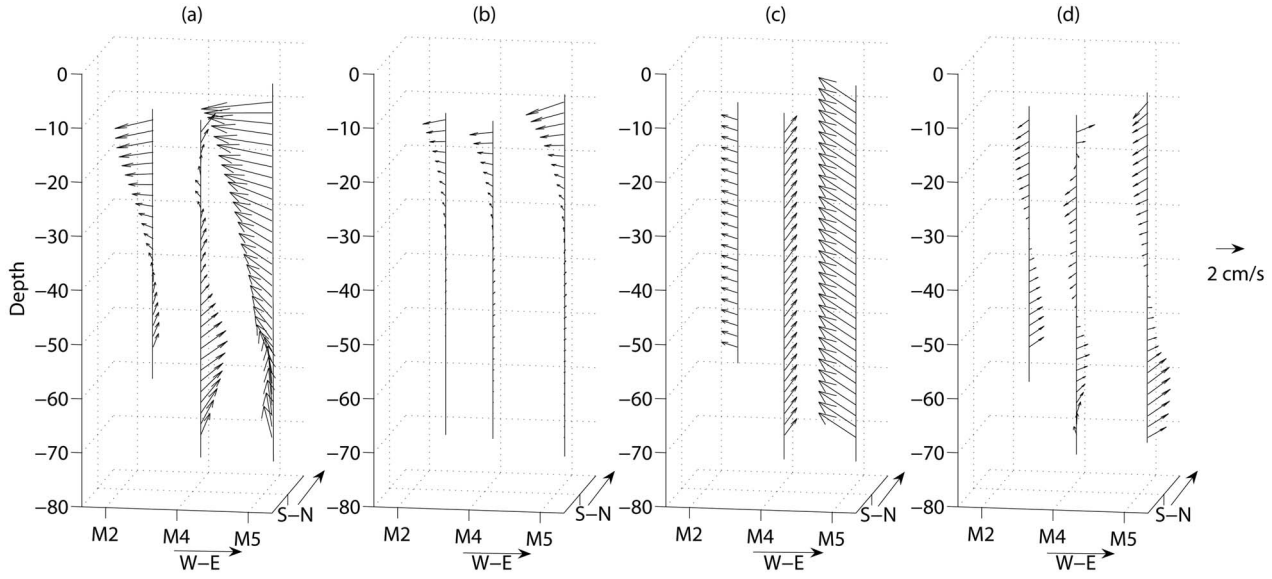

Figure 10. Time-averaged (a) residual current, (b) Ekman current, (c) barotropic current, and (d) baroclinic current at M2, M4, and M5.

Table 3. Current Speed at Four Mooring Stations

Station	Mean Barotropic Current (cm s^{-1})	Ekman Current (cm s^{-1})	Depth-Averaged Absolute Baroclinic Current (cm s^{-1})
M2	2.40, −2.32 (Zonal), 0.63 (Meridional)	0.78 (Depth averaged), 3.25 (Surface)	1.80
M4	2.54, −0.22 (Zonal), 2.52 (Meridional)	0.64 (Depth averaged), 3.95 (Surface)	1,21
M5	7.46, −6.56 (Zonal), 3.56 (Meridional)	0.67 (Depth averaged), 4.10 (Surface)	2.16
M6	1.22, −0.35 (Zonal), 1.17 (Meridional)	0.68 (Depth averaged), 4.18 (Surface)	0.74

[21] Figure 11 shows the mean residual current (Figure 11a), the Ekman current (Figure 11b), the barotropic current (Figure 11c), and the baroclinic current (Figure 11d) at station M6 which was located near the center of the northern end of the trough (Figure 2). The current speed was small at M6 and around 2 cm s^{-1}, but basically northward in the whole water depth. This northward current also supports that the YSWC flows northeastward in the north of 35N with slightly downslope movement as we discussed in sections 2 and 3. The Ekman current and baroclinic current became more important in the surface layer where they were directed southward.

4.4. The Time Series of Mooring Currents

[22] The northward flow was evident not only in the time mean field as shown above but dominated during the whole observation period. Figure 12 shows the time series of wind (the adjacent nine grid points mean of QuikSCAT observations), the barotropic current (depth averaged) and the baroclinic current of 10m, 30m, 50m and bottom (removing barotropic component) at mooring station M5, where the warm/salty water core was located. The barotropic current was mostly northward except in a few days when it reversed to weakly southward. This southward flow seemed to be related with the weak northerly wind such as during 19–23 December 2006 or 1–4 January 2007. The northward current intensified after strong northerly wind burst. In 27 December 2006, the strong northwesterly wind of 15 m s^{-1} induced a northwestward current of more than 30 cm s^{-1} in the following day, which was the maximum current speed during the observation. After 4 January 2007, the northerly wind became steady and then barotropic current was always northwestward with the speed around 10 cm s^{-1}. The baroclinic current at M5 also varied with the changing of wind. It showed a clear vertical shear and surface and bottom intensification. In the surface layer of 10m depth, the baroclinic current was basically southward and often reached 10 cm s^{-1}. The northward baroclinic current was dominant in the bottom layer with maximum speed more than 10 cm s^{-1}. This intensified northward current in the bottom layer may be responsible for the formation of high-salinity core with inverse temperature as observed in the lower layer in the routine section and in situ observations. The baroclinic current in the intermediate layers, such as 30 and 50 m shown in Figure 12, was very weak during the whole observation. After 4 January 2007, when the northerly wind and northwestward barotropic current became steady, the baroclinic currents in surface and bottom layers were also weak. All the above further confirm our assertion that the YSWC was induced mainly by the barotropic current. At mooring station M6 near the northern end of YST, the northward current was still clearly shown. Figure 13 shows the time series of wind, the barotropic current and the baroclinic current of 10 m, 30 m, 50 m, and bottom at M6. Like M5, the barotropic current time series at M6 was basically northward, with occasionally southward when the

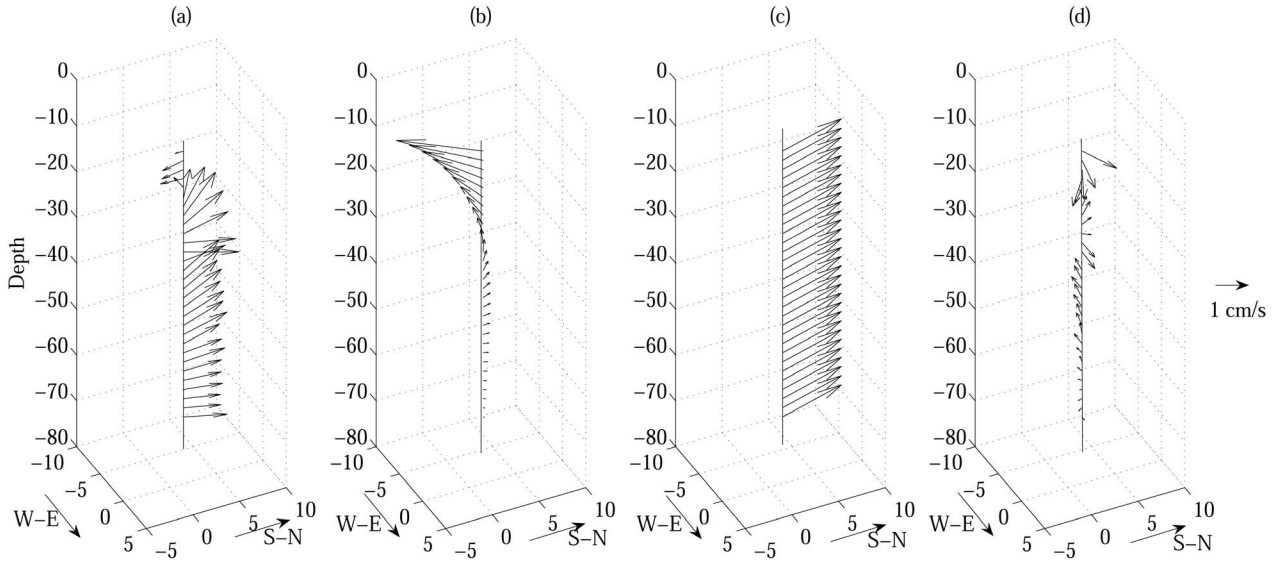

Figure 11. The same as Figure 10 but for M6.

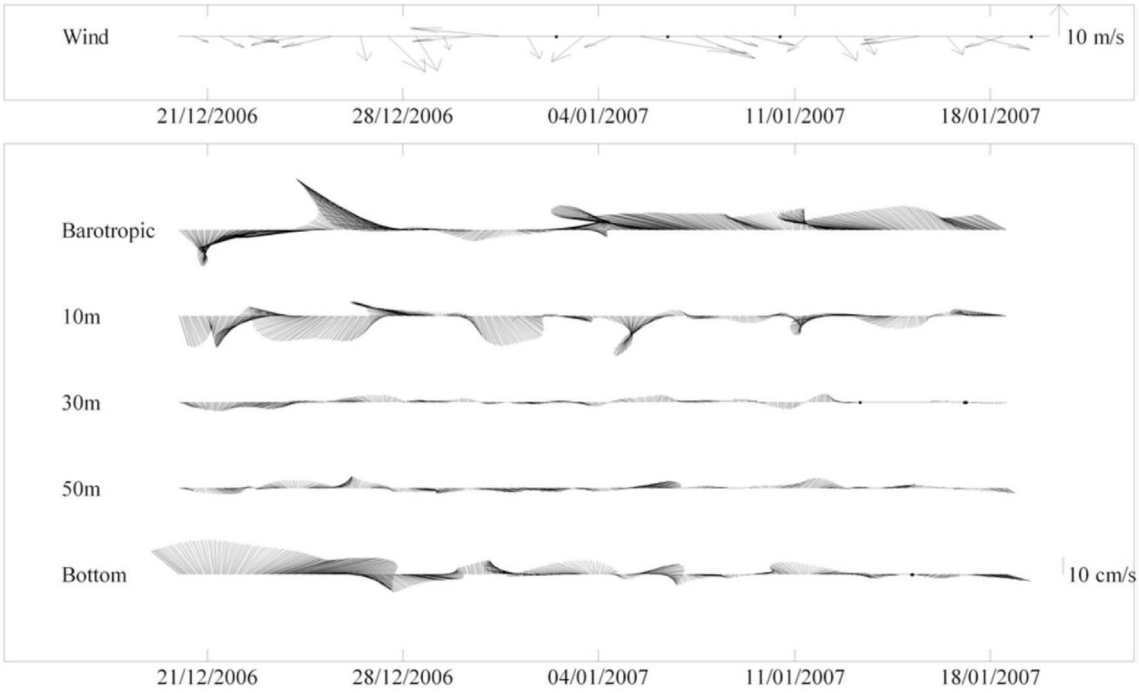

Figure 12. Time series of wind (the adjacent nine grid points mean of QuikSCAT observations); the barotropic current (depth averaged); and the baroclinic current of 10 m, 30 m, 50 m, and bottom (removing barotropic component) at mooring station M5.

northerly wind was weaken. But the current speed at M6 was much weaker than that at M5. The maximum northwestward current occurred in 8 January 2010, after the strong northwesterly wind burst in previous day, was less than 5 cm s^{-1}. There was only surface intensification of baroclinic current at M6 as shown in 10 m layer observations, which showed a strong southward baroclinic current. The very weak baroclinic current in the lower layer, such as 30 m, 50 m,

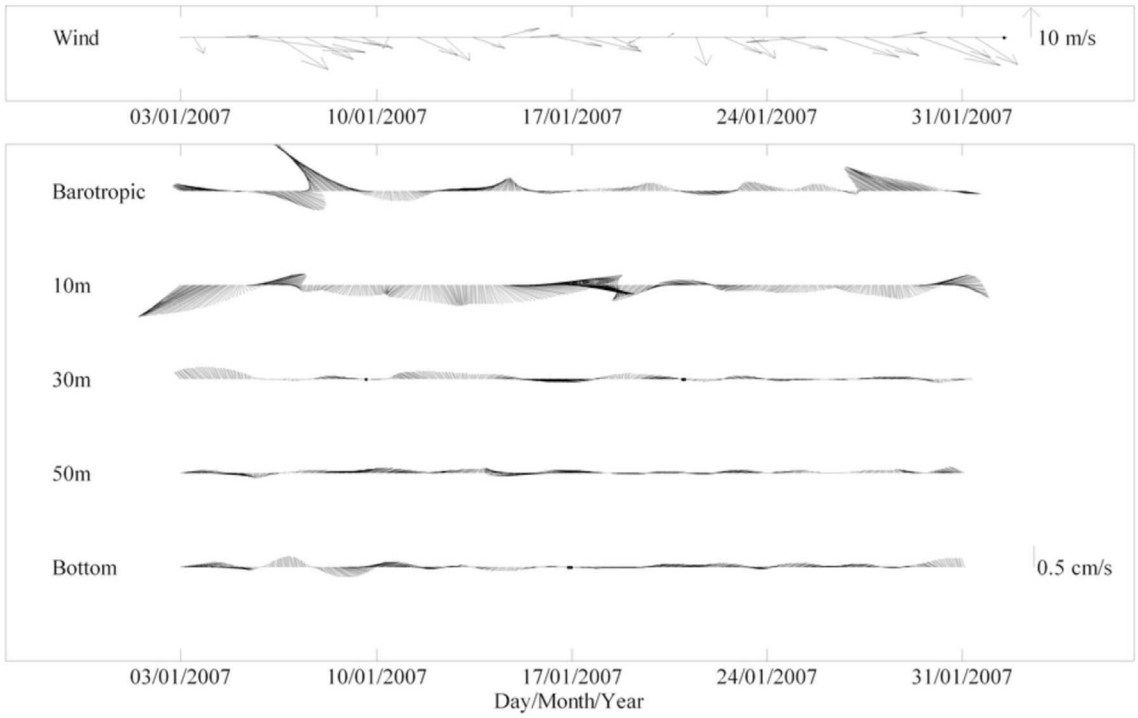

Figure 13. The same as Figure 12 but for M6.

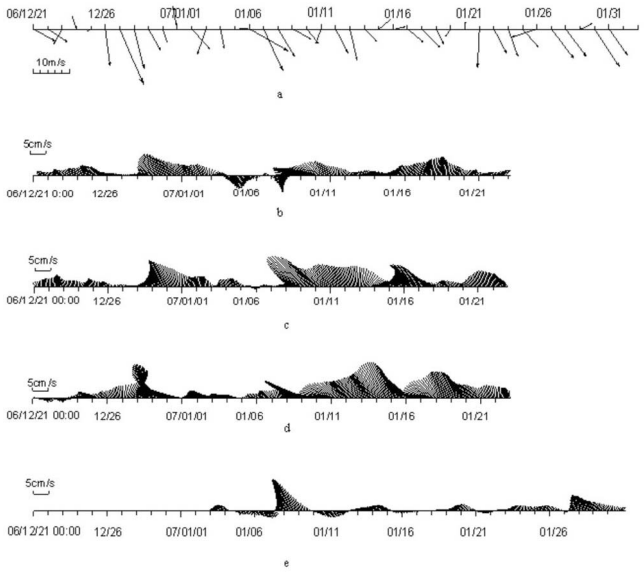

Figure 14. The time series of observed daily wind in 2006–2007 winter in north Yellow Sea (averaged in the box from 34°N to 38°N, 122°E to 124°E) from (a) QuikSCAT data and near bottom residual current in station (b) M2, (c) M4, (d) M5, and (e) M6.

and bottom, also suggests the dominance of barotropic current.

[23] It should be noted here that since the QuikSCAT observations only have daily data, we cannot remove the Ekman current in our mooring current series with 5 min interval. Our barotropic and baroclinic current series shown in Figures 12 and 13 always contained the Ekman component. The Ekman current speed reaches its maximum value in the surface or bottom layer and may have strong effect on the surface baroclinic and barotropic current series. According to our Ekman model estimation, the mean Ekman current in the surface at these mooring stations was about 4 cm s^{-1} (Table 3). At M5, barotropic and surface baroclinic currents often exceeded 10 cm s^{-1}, so the effect of Ekman current seems to be secondary. But at M6, the barotropic and baroclinic currents were weak and the Ekman current could be dominant in the surface layer. In fact, the 10m baroclinic current at M6 seemed always on the right-hand of surface wind, consistent with the Ekman current. At M2 and M4, where the current were weak, the effect of Ekman current was also important in the barotropic and baroclinic time series of current field (figures not shown here). To avoid the effect of Ekman current, we choose the residual current series near bottom layer, which are far below the Ekman layer, to show the existence of YSWC. Figure 14 is the time series of observed daily wind in 2006–2007 winter in the northern Yellow Sea (averaged in the box from 34°N to 38°N, 122°E to 124°E) from QuikSCAT data (Figure 14a) and near bottom residual current in station M2 (Figure 14b), M4 (Figure 14c), M5 (Figure 14d), and M6 (Figure 14e). Compared with the local wind from QuikSCAT observations, the variances of currents in these mooring stations corresponded well with the surface wind variations, with about 1–2 day delay. The observed northward current intensified after a strong northerly wind burst, consistent with the finding of previous studies [*Hsueh*, 1988; *Hsueh and Yuan*, 1997; *Mask et al.*, 1998; *Jacobs et al.*, 2000; *Riedlinger and Jacobs*, 2000]. Despite temporal variation of velocity in response to fluctuations in surface wind stress, the velocity measured at all stations on the western side of the trough (M2, M4, and M5) was consistently northward for the whole period. This demonstrated unambiguously that there is a steady northward flow along the western side of the YST in winter. This is perhaps the most definite and direct confirmation of the existence of the YSWC to date. The velocity measured at station M6, which was located near the center of the northern end of the trough, showed more fluctuations and was more responsive to synoptic wind stress forcing. This could explain to some extent why previous observations in the center or along the eastern side of the YST failed to observe a steady northward current.

[24] The main objective of this paper is to present new observations and to demonstrate the existence of the YSWC on the western side of the YST. We have examined some dynamical processes that could be responsible for the westward displacement of the YSWC core. Our preliminary examination indicates that interplay between vorticity fluxes from wind stress and friction, together with bathymetry, could explain the westward displacement of the warm current core. The results will be reported later when the study is completed.

5. Summary

[25] The existence of the YSWC has been a subject of debate. The presence of warm and salty water along the YST in the winter is evident both in in situ and remote sensing observations. Yet there had been no confirmation of the YSWC from direct current measurements. In addition, hydrographic observations had been scarce on the western side of the trough where the YSWC core is located. This lack of observational evidence has prompted several hypotheses about the cause of the observed warm water intrusion. Alternative mechanisms include frontal mixing, eddy flux, barotropic responses to synoptic time scale wind bursts, convective mixing, etc. It is noted that most direct current measurements available in previous studies were made on the center and eastern sides of the YST. Yet, the core of warm water intrusion was evidently on the western side of the trough where observations have been extremely scarce. In this study, we present results from a large-scale observational study made by a coordinated effort involving three Chinese research vessels in the winter of 2006–2007. The existence of the YSWC on the western side of the YST is confirmed unambiguously. The ADCP moorings show a steady northward YSWC in the western YST during the 45 day observation with the maximum mean speed of more than 5 cm s^{-1}. The warm water intrusion starts roughly at the center of the trough at the entrance of the YST. South of 35°N it moves gradually upslope and westward. Our analysis shows that the barotropic current makes a greater contribution for the YSWC and may be responsible for the cross shelf and westward shift of YSWC, while Ekman and baroclinic velocities play an important but secondary role. Thirty one years of continuous routine observations in the

western YS and a 24 year satellite SST record from the YS were also used in this study. These clearly show that the core of the warm water intrusion moves upslope toward the west as the YSWC penetrates further along the YST south of 35°N.

[26] **Acknowledgments.** The authors have been supported by China's National Basic Research Priorities Programmer (2007CB411804 and 2005CB422303), the Ministry of Education's 111 Project (B07036), the Program for New Century Excellent Talents in University (NECT-07-0781), and the China National Science Fundation (40976004, 40921004. and 40930844). J.Y. is supported by the U.S. National Science Foundation and the Woods Hole Oceanographic Institution's Coastal Ocean Institute. We are very grateful to Magdalena Andres (WHOI) who thoroughly reviewed the manuscript and gave many valuable comments and suggestions. Her help has considerably improved the manuscript.

References

Beardsley, R. C., R. Limeburner, H. Yu, and G. A. Cannon (1985), Discharge of the Changjiang (Yangtze River) into the East China Sea, *Cont. Shelf Res.*, *4*, 57–76, doi:10.1016/0278-4343(85)90022-6.

Beardsley, R. C., R. Limeburner, K. Kim, and J. Candela (1992), Recent advances in ocean-circulation research on the Yellow Sea and East China Sea shelves 583 Lagrangian flow observations in the East China, Yellow, and Japan seas, *Mer*, *30*, 297–314.

Brink, K. H. (1998), Deep-sea forcing and exchange processes, in *The Sea*, vol. 10, *The Global Coastal Ocean: Processes and Methods*, edited by K. H. Brink and A. R. Robinson, pp. 151–167, John Wiley, New York.

Duchon, C. E. (1979), Lanczos filtering in one and two dimensions, *J. Appl. Meteorol.*, *18*, 1016–1022, doi:10.1175/1520-0450(1979)018<1016:LFIOAT>2.0.CO;2.

Gao, G., C. Qian, X. Bao, and M. Shi (2001), Difference between the PFSST and the in-situ data in East China Sea (in Chinese), *Acta Oceanol. Sin.*, *23*, 121–126.

Guan, B. (1994), Patterns and structures of the currents in Bohai, Huanghai and East China seas, in *Oceanology of China Seas*, vol. 1, edited by Z. Di et al., pp. 17–26, Kluwer Acad., Norwell, Mass.

Guan, B., and S. Chen (1964), Current system in the marginal seas of China (in Chinese), *Natl. Oceanogr. Compr. Surv. Rep.*, *5*, 1–85.

Guo, B., et al. (2000), Seasonal variation of water exchange between the Yellow Sea and the East China Sea (in Chinese), *Acta Oceanol. Sin.*, *22*, 12–23.

Guo, B., et al. (2004), *The Ocean Environment of the Marginal Seas Adjacent to China*, 446 pp., China Ocean Press, Beijing.

Hsueh, Y. (1988), Recent current observations in the eastern Yellow Sea, *J. Geophys. Res.*, *93*, 6875–6884, doi:10.1029/JC093iC06p06875.

Hsueh, Y., and D. Yuan (1997), A numerical study of the currents, heat advection and sea level fluctuations in the Yellow Sea in winter 1986, *J. Phys. Oceanogr.*, *27*, 2313–2326, doi:10.1175/1520-0485(1997)027<2313:ANSOCH>2.0.CO;2.

Hsueh, Y., R. D. Romea, and P. W. deWitt (1986), Windertime winds and sea-level fluctuations in the northeast China Sea. Part II: Numerical model, *J. Phys. Oceanogr.*, *16*, 241–261, doi:10.1175/1520-0485(1986)016<0241:WWACSL>2.0.CO;2.

Huang, D., X. Fan, D. Xu, Y. Tong, and J. Su (2005), Westward shift of the Yellow Sea warm salty tongue, *Geophys. Res. Lett.*, *32*, L24613, doi:10.1029/2005GL024749.

Ichikawa, H., and R. C. Beardsley (2002), The current system in the Yellow and East China seas, *J. Oceanogr.*, *58*, 77–92, doi:10.1023/A:1015876701363.

Isobe, A. (2008), Recent advances in ocean-circulation research on the Yellow Sea and East China Sea shelves, *J. Oceanogr.*, *64*, 569–584, doi:10.1007/s10872-008-0048-7.

Jacobs, G. A., H. B. Hur, and S. K. Riedlinger (2000), Yellow and East China seas response to winds and currents, *J. Geophys. Res.*, *105*, 21,947–21,968, doi:10.1029/2000JC900093.

Kilpatrick, K. A., G. P. Podesta, and R. Evans (2001), Overview of the NOAA/NASA Advanced Very High Resolution Radiometer Pathfinder algorithm for sea surface temperature and associated matchup database, *J. Geophys. Res.*, *106*, 9179–9197, doi:10.1029/1999JC000065.

Lie, H.-J. (1986), Summertime hydrographic features in the southeastern Hwanghae, *Prog. Oceanogr.*, *17*, 229–242, doi:10.1016/0079-6611(86)90046-7.

Lie, H.-J., C.-H. Choi, J.-H. Lee, S. Lee, and Y. Tang (2000), Seasonal variation of the Cheju Warm Current in the northern East China Sea, *J. Oceanogr.*, *56*, 197–211, doi:10.1023/A:1011139313988.

Lie, H.-J., C.-H. Cho, J.-H. Lee, and S. Lee (2001), Does the Yellow Sea Warm Current really exist as a persistent mean flow?, *J. Geophys. Res.*, *106*, 22,199–22,210, doi:10.1029/2000JC000629.

Lie, H.-J., C.-H. Cho, and S. Lee (2009), Tongue-shaped frontal structure and warm water intrusion in the southern Yellow Sea in winter, *J. Geophys. Res.*, *114*, C01003, doi:10.1029/2007JC004683.

Liu, W. T. (2002), Progress in scatterometer application, *J. Oceanogr.*, *58*, 121–136, doi:10.1023/A:1015832919110.

Ma, J., F. Qiao, C. Xia, and C. S. Kim (2006), Effects of the Yellow Sea Warm Current on the winter temperature distribution in a numerical model, *J. Geophys. Res.*, *111*, C11S04, doi:10.1029/2005JC003171.

Mask, A. C., J. J. O'Brien, and R. Preller (1998), Wind-driven effects on the Yellow Sea Warm Current, *J. Geophys. Res.*, *103*, 30,713–30,729, doi:10.1029/1998JC900007.

Nitani, H. (1972), Beginning of the Kuroshio, in *Kuroshio—Its Physical Aspects*, edited by H. Stommel and K. Yoshida, pp. 353–369, Univ. of Tokyo Press, Tokyo.

Park, Y.-H. (1986), Water characteristics and movements of the Yellow Sea Warm Current in summer, *Prog. Oceanogr.*, *17*, 243–254, doi:10.1016/0079-6611(86)90047-9.

Price, J. F., and M. A. Sundermeyer (1999), Stratified Ekman layers, *J. Geophys. Res.*, *104*, 20,467–20,494, doi:10.1029/1999JC900164.

Riedlinger, S. K., and G. A. Jacobs (2000), Study of the dynamics of wind-driven transports into the Yellow Sea in winter, *J. Geophys. Res.*, *105*, 28,695–28,708, doi:10.1029/2000JC900127.

Su, J., et al. (2005), A coupled ice-ocean model for the Bohai Sea: Part II. Case study, *Acta Oceanol. Sin.*, *24*, 54–67.

Tang, Y., E. Zou, and H.-J. Lie (2001), On the origin and path of the Huanghai Warm Current during winter and early spring (in Chinese with English abstract), *Acta Oceanol. Sin.*, *23*, 1–12.

Teague, W. J., and G. A. Jacobs (2000), Current observations on the development of the Yellow Sea Warm Current, *J. Geophys. Res.*, *105*, 3401–3411, doi:10.1029/1999JC900301.

Uda, M. (1934), Hydrographical research on the normal monthly conditions in the Japan Sea, the Yellow Sea, and the Okhotsk Sea (in Japanese), *J. Imp. Fish. Exp. Stn.*, *5*, 191–236.

Uda, M. (1936), Results of simultaneous oceanographic investigations in the Japan Sea and its adjacent waters during October and November, 1933 (in Japanese), *J. Imp. Fish. Exp. Stn.*, *7*, 91–151.

Xie, S. P., J. Hafner, Y. Tanimoto, W. T. Liu, H. Tokinaga, and H. Xu (2002), Bathymetric effect on the winter sea surface temperature and climate of the Yellow and East China seas, *Geophys. Res. Lett.*, *29*(24), 2228, doi:10.1029/2002GL015884.

Yu, F., Z. Zhang, X. Diao and J. Guo (2010), The observation evidence of the Yellow Sea Warm Current, *Oceanol. Limnol. Sin.*, *28*, 677–683, doi:10.1007/s00343-010-0006-2.

Yuan, D., J. Zhu, C. Li, and D. Hu (2008), Cross-shelf circulation in the Yellow and East China seas indicated by MODIS satellite observations, *J. Mar. Syst.*, *70*, 134–149, doi:10.1016/j.jmarsys.2007.04.002.

Yuan, Y. C., and J. L. Su (1984), Numerical modeling of the circulation in the East China Sea, in *Ocean Hydrodynamics of Japan and East China Seas*, *Elsevier Oceanogr. Ser.*, vol. 39, edited by T. Ichiye, pp. 167–186, doi:10.1016/S0422-9894(08)70299-X, Elsevier, New York.

J. Guo and Z. Zhang, Key Laboratory of Marine Science and Numerical Modeling, First Institute of Oceanography, State Oceanic Administration, 6 Xianxialing Rd., Qingdao 266061, China.

X. Lin, X. Song, Y. Yin, and X. Zhang, Physical Oceanography Laboratory, Ocean University of China, Qingdao 266003, China. (linxiaop@ouc.edu.cn)

J. Yang, Department of Physical Oceanography, Woods Hole Oceanographic Institution, Clark 303A, MS 21, Woods Hole, MA 02543, USA.